Proceedings of the Canadian Society for Mechanical Engineering International Congress
32nd Annual Conference of the Computational Fluid Dynamics Society of Canada
Canadian Society of Rheology Symposium
CSME-CFDSC-CSR 2025
May 25–28, 2025, Montréal, Québec, Canada

EFFICIENT MODELLING OF HIGH REYNOLDS NUMBER INCOMRPESSIBLE FLOWS IN A Q-SUBDOMAIN BY FEM

Shudong Yu
Department of Mechanical, Industrial and Mechatronics Eng., Toronto Metropolitan University, Toronto, Canada
syu@torontomu.ca

Abstract— Four-node quadratic elements are proposed in this paper to simulate 2D incompressible pressure-independent flows in a Q-subdomain. The Galerkin principle is used to formulate the governing equations of the nodal variables – the stream function and its spatial derivatives. In the process of domain integrations, large eddies are directly modelled while the effects of small eddies are captured using the shape functions. Numerical results, obtained the proposed approach for the lid-driven flow in a square cavity, show good agreement with those in the literature for high Re flows.

Keywords - incompressible flows, finite element method, stream function, incremental load method.

I. INTRODUCTION

For incompressible flows, the pressure is not a full variable because it does not have its own valid partial differential equation. In this paper, the incompressible flows are classified into the pressure-independent flows and the pressure-dependent flows. To eliminate the need for iterations to satisfy the incompressibility constraint, the velocities are obtained from the curl of the stream function [1].

For the pressure-independent flows, the normal velocities on the boundaries of the fluid domain of interest are everywhere zero. There are no exchanges of mass between the modelled fluid domain and its non-modelled surroundings. Typical examples of this type of flows are flows in a cavity or closure. The pressure is strictly a flow-induced variable and can be determined by solving the Poisson equation, which is derived from the NS equations by simply taking the divergence of the momentum equations. The Galerkin principle can be used to formulate the weak form of integral equation and eliminate the domain and boundary pressure effects by means of the integration-by-part scheme and application of Green's lemma.

Flow behaviors can change considerably in the spatial and temporal domains under time-invariant and time-varying excitations. To simulate long-term behaviors of flows, e.g., steady, unsteady and turbulent, it is essential to obtain the initial flow, which satisfies the steady NS equations for the desired initial conditions.

The incremental load method is used to compute the initial flow field, characterized by the Reynolds number $R_{e,0}$, by ramping up all excitations to their desired initial values in steps from the quiescent state. The single non-dimensional load parameter, varying from 0 to 1 on a 4-5-6-7 polynomial, is employed as a scaler. The mesh size and the number of load steps are used to control the accuracy. To validate the $R_{e,0}$-compatible mesh and load steps, the kinetic energies of the domain of interest are computed for each load step until R_e reaches $R_{e,0}$. The K-R_e curve is expected to a smooth curve without peculiarities.

Once the initial flow field is established, the validated finite mesh can be used to solve the dynamic NS equations with the temporal terms for simulating long-term flow behavior. If the terminal flow is steady, then the initial flow is the flow being sought.

In this paper, the methodology is presented for 2D pressure-independent initial incompressible flows. Numerical results are presented only for the well-known lid-driven flow with two Reynolds numbers: 10,000 and 100,000.

II. MATHEMATICAL FORMUALTION

A. NS Equations

In the Cartesian coordinate system, the 2D incompressible flows without considering heat transfer are governed by the following NS equations for velocity components v_x and v_y, and pressure p

$$\underbrace{\rho\left(v_x\frac{\partial v_x}{\partial x}+v_y\frac{\partial v_x}{\partial y}\right)-\left(\frac{\partial \sigma_{xx}}{\partial x}+\frac{\partial \sigma_{xy}}{\partial y}\right)}_{L_x}+\frac{\partial p}{\partial x}=0 \qquad (1)$$

$$\underbrace{\rho\left(v_x\frac{\partial v_y}{\partial x}+v_y\frac{\partial v_y}{\partial y}\right)-\left(\frac{\partial \sigma_{yx}}{\partial x}+\frac{\partial \sigma_{yy}}{\partial y}\right)}_{L_y}+\frac{\partial p}{\partial y}=0 \tag{2}$$

$$\frac{\partial v_x}{\partial x}+\frac{\partial v_y}{\partial y}=0 \tag{3}$$

B. Galerkin Potential

With help of a single stream function ψ, the velocity field, which satisfies (3), is defined by

$$v_x=\frac{\partial \psi}{\partial y}, v_y=-\frac{\partial \psi}{\partial x} \tag{4}$$

The following Galerkin potential, which is equivalent to the strong form of the NS equations, is employed to formulate the governing equations of the nodal variables, suited for the finite element method

$$\Pi=\iint_\Omega \frac{\partial \psi^*}{\partial y}\left(L_x+\frac{\partial p}{\partial x}\right)dA+\iint_\Omega\left(-\frac{\partial \psi^*}{\partial x}\right)\left(L_y+\frac{\partial p}{\partial y}\right)dA=0 \tag{5}$$

where ψ* is the arbitrary and admissible stream function.

To eliminate the domain pressure and better condition the governing equations in the subsequent finite element modelling, the integration-by-part scheme is employed on the deviatoric stress terms and the pressure gradient terms in the Galerkin integral. Utilizing the incompressibility constraint and Green's lemma, the Galerkin potential is rewritten as the sum of the domain and boundary integrals as follows

$$\begin{aligned}\Pi=&\iint_\Omega \rho\left\{\frac{\partial \psi^*}{\partial x}\frac{\partial \dot{\psi}}{\partial x}+\frac{\partial \psi^*}{\partial y}\frac{\partial \dot{\psi}}{\partial y}\right\}dA\\&+\iint_\Omega \frac{\partial \psi^*}{\partial x}\rho\left(\frac{\partial \psi}{\partial y}\frac{\partial^2\psi}{\partial x^2}-\frac{\partial \psi}{\partial x}\frac{\partial^2\psi}{\partial x\partial y}\right)dA\\&+\iint_\Omega \frac{\partial \psi^*}{\partial y}\rho\left(\frac{\partial \psi}{\partial y}\frac{\partial^2\psi}{\partial x\partial y}-\frac{\partial \psi}{\partial x}\frac{\partial^2\psi}{\partial y^2}\right)dA\\&+\iint_\Omega \mu\left\{\left(\frac{\partial^2\psi^*}{\partial y^2}-\frac{\partial^2\psi^*}{\partial x^2}\right)\left(\frac{\partial^2\psi}{\partial y^2}-\frac{\partial^2\psi}{\partial x^2}\right)+4\frac{\partial^2\psi^*}{\partial x\partial y}\frac{\partial^2\psi}{\partial x\partial y}\right\}dA\\&-\oint_\Gamma v_n^*(\sigma_{nn}-p)ds-\oint_\Gamma v_s^*\sigma_{sn}ds=0\end{aligned} \tag{6}$$

where μ is dynamic viscosity; ρ is density; Ω is the fluid domain; Γ is the fluid boundary. For pressure-intendent flows, the boundary integral in connection with the pressure and the normal deviatoric stress vanishes.

C. Geometric Mapping and Meshing

A two-dimensional domain formed by no more than four pieces of continuous curves with four or fewer singular points, termed as a Q-subdomain, can be mapped into a perfect dimensionless square of dimensions 2×2. For example, a quadrilateral domain of four straight edges, shown in Fig.1, can be mapped into the parent square from the following transformation

$$x=\left[N(\alpha,\beta)\right]_G\{\bar{x}\}, y=\left[N(\alpha,\beta)\right]_G\{\bar{y}\} \tag{7}$$

where $[N]_G$ is the mapping function array; α and β are non-dimensional coordinates; $\{\bar{x}\}$ and $\{\bar{y}\}$ are the Cartesian coordinates of the four key points,

$$[N]_G=\frac{1}{4}\begin{bmatrix}1 & \alpha & \beta & \alpha\beta\end{bmatrix}\begin{bmatrix}1 & 1 & 1 & 1\\ -1 & 1 & 1 & -1\\ -1 & -1 & 1 & 1\\ 1 & -1 & 1 & -1\end{bmatrix} \tag{8}$$

$$\{\bar{x}\}=\begin{Bmatrix}x_1\\x_2\\x_3\\x_4\end{Bmatrix}, \{\bar{y}\}=\begin{Bmatrix}y_1\\y_2\\y_3\\y_4\end{Bmatrix} \tag{9}$$

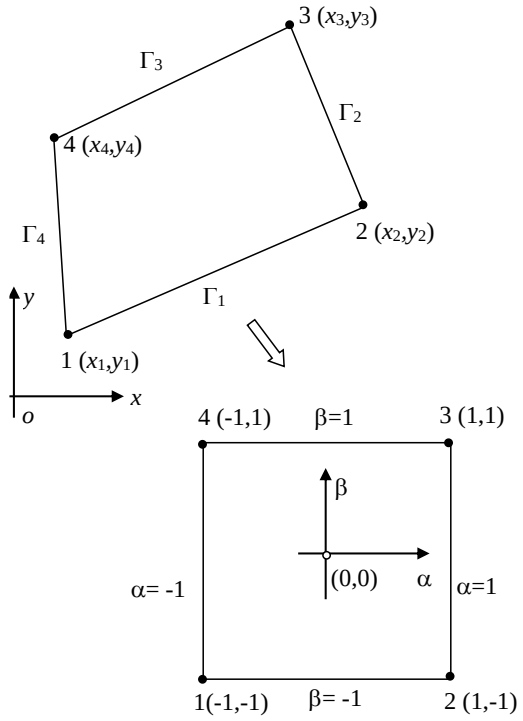

Fig.1 Mapping of a general quadrilateral domain through shape function array and four control points

Once a Q-subdomain is mapped into a dimensionless square, the finite element mesh can be done very easily on the square. Four node quadrilateral elements are used in this paper to mesh a Q-subdomain. To address the complex flow behaviour in the boundary region, one division of elements, adjacent to the four boundaries, is subdivided into a few sublayers. The FE model shown in Fig.2 consists of 8×8 uniform domain elements, 160 boundary elements, and 100 corner elements.

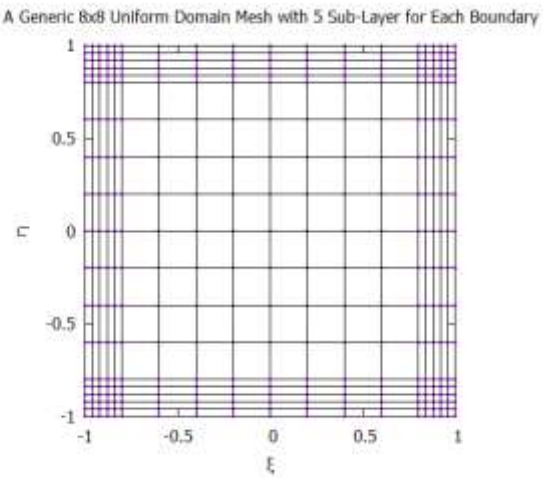

Fig.2 A uniform and non-uniform FE mesh with 361 nodes

Following the standard finite element procedure in [2] and the typical formation of the admissible disturbance, within a finite element region, the stream function and the admissible stream function are assumed to vary with the non-dimensional coordinates (ξ,η) in accordance with the same shape function row-array in the parent square $[-1,1;-1,1]$ as follows

$$\psi_e(x,y) = \left[\hat{N}(\xi,\eta)\right]\{\hat{\psi}\}_e \tag{10}$$

$$\psi_e^*(x,y) = \left[\hat{N}(\xi,\eta)\right]\{\hat{\psi}^*\}_e \tag{11}$$

where $\{\hat{\psi}\}_e$ and $\{\hat{\psi}^*\}_e$ are the actual and admissible element nodal variable arrays, respectively.

Carrying out the integrals over all finite element regions and assembling the contributions of all elements N_e, the Galerkin potential is written as

$$\Pi = \sum_{e=1}^{N_e} \Pi_e\left(\{\hat{\psi}^*\},\{\hat{\psi}\}\right) \tag{12}$$

where $\{\hat{\psi}\}$ and $\{\hat{\psi}^*\}$ are the actual and admissible global nodal arrays, respectively.

D. Solution Scheme

A set of nonlinear algebraic equations of $\{\hat{\psi}\}$ may be obtained by invoking the arbitrariness of $\{\hat{\psi}^*\}$. An incremental method is employed to transform the nonlinear equations into the linear algebraic equations with varying coefficients. With this method, the desired flow is ramped up incrementally in N load steps from the quiescent state without iterations. With the help of a non-dimensional load parameter θ, R_e is varied from zero to $R_{e,0}$ in N steps, $[0,\Delta\theta],[\Delta\theta,2\Delta\theta],\ldots$, and $[(N-1)\Delta\theta,1]$, here $\Delta\theta = 1/N$, according the following profile

$$R_e = R_{e,D}\left(35\theta^4 - 84\theta^5 + 70\theta^6 - 20\theta^7\right) \tag{13}$$

Within a typical load step, $[\theta_r, \theta_{r+1}]$, the incremental global nodal variable array is sought by solving the following recursive algebraic equations

$$\left[\hat{K}\left(\{\hat{\psi}\}_r\right)\right]\{\Delta\hat{\psi}\}_{r\to r+1} = \{\hat{Q}\}_{r+1} + \{\hat{R}\}_{r+1} \tag{14}$$

where $\{\hat{\psi}\}_r$ is the known global nodal variable array at the start of a load step; $\{\Delta\hat{\psi}\}_{r\to r+1}$ is the incremental array to be sought; $\{\hat{Q}\}_{r+1}$ is the known excitation array. The boundary reaction array $\{\hat{R}\}_{r+1}$ is unknown. A solution to (14) requires boundary conditions.

For pressure-independent flows, the normal velocities everywhere on the boundaries are zero. The penalty method can be used to treat the boundary condition in the normal direction.

In the tangential direction, the boundary can be responsive to the flow. For the no-slip condition, the penalty method can also be employed to deal with the prescribed tangential velocity. For smooth wall condition, the components of the reaction array associated with the tangential nodal velocities vanish. For general tangential conditions, a tangential response modulus can be introduced to correlate the boundary shear stress to the tangential velocity. The corresponding components in the reaction array can be determined by carrying the boundary integral.

III. NUMERICAL RESULS AND DISCUSSIONS

The proposed approach is applied to a well-studied lid-driven flow problem in a cavity [1] shown in Fig. 3. The flow is driven by a single source of excitation - the sliding of the top lid in the tangential direction. The lid velocity U is varied to achieve any desired value of R_e number. The initial flow under constant lid velocity is found using the proposed.

Spatial distributions of eddies and their sizes can vary considerably as the flow is ramped up from the quiescent state to the initial state characterized by the initial value of $R_{e,0}$. For this reason, a fixed mesh size controlled by the number divisions of the cavity in the two coordinate directions is decided from $R_{e,0}$ in order to capture the spatial characteristics of the targeted initial and ensuing flow.

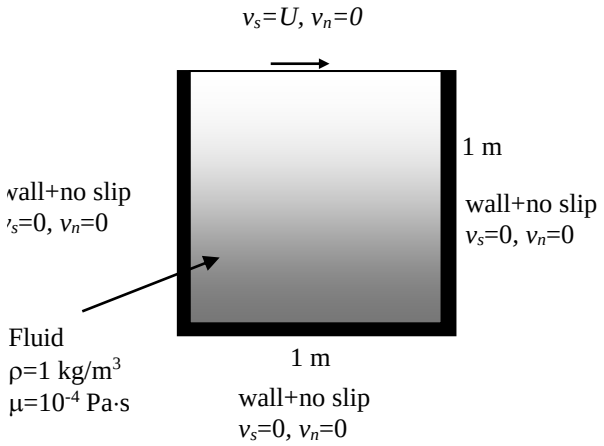

Fig. 3 Lid-driven flow in a square cavity

As the Re number increases, the shear stresses near a boundary can experience rapid changes in the normal direction.

For lid-driven flows in a 1 m ×1 m square cavity, the shear stresses for Re=100,000 are discontinuous at a distance of about 3 mm from the top and bottom faces where two sharp cusps occur. To simulate high Re number flows in a cavity with confidence, reasonably small size elements are needed to capture the domain eddies. Smaller sizes of elements are needed in the boundary region to capture the precise locations of the shear stress discontinuities. In addition, the load steps should be large to capture significant advective effects. Since the exact locations of the cusps are not known a priori, a qualification run is needed to verify the appropriateness of the domain mesh size, the boundary mesh size and load steps. Numerical results show that inappropriate mesh sizes and/or insufficient load steps cause the kinetic energy to vary with the Re numbers abnormally.

The flow variables were computed using two schemes. In scheme 1, the cavity is meshed with 32×32 elements; 22×22 domain elements; the boundary division is subdivided into 5 layers; the load steps is 32; the target initial Reynolds number is 10,000. In scheme 2, the cavity is meshed with 66×66 elements; 56×56 are domain elements; the boundary division is subdivide into 6 layers; the number of load steps is 66; the target initial Reynolds number is 100,000.

The variations of the kinetic energies with the Reynolds numbers shown in Fig. 4 and Fig. 5 indicate that the two modelling schemes are valid.

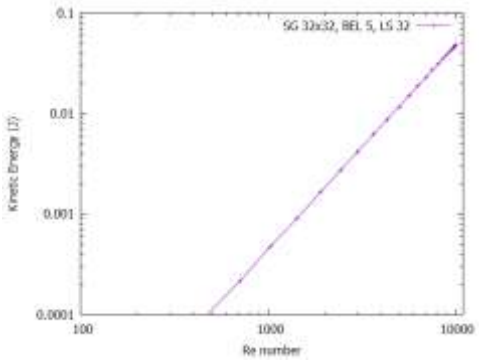

Fig. 4 Kinetic energy vs Reynolds numbers with a target value 10,000

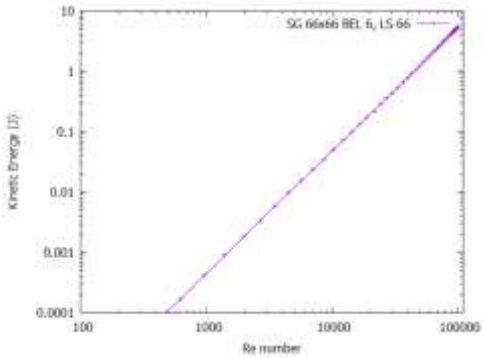

Fig. 5 Kinetic energy vs Reynolds numbers with a target value 100,000

The computed *x*-velocities of the vertical centreline in Fig. 6 are in good agreement with those of [1] for Re=10,000. the tangential velocity cusp appears at 9 mm from the bottom wall.

Results shown in Fig. 7 show the occurrence of the tangential velocity cups at 3 mm from the bottom wall. The out-most boundary layer element must have the smallest size of 3 mm to precisely capture the cusp.

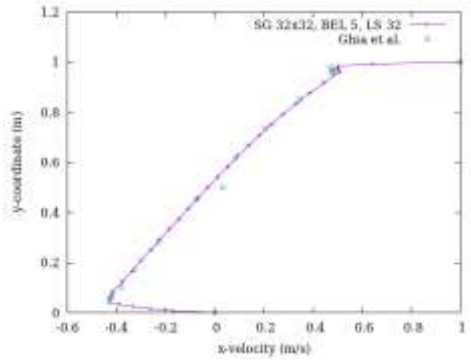

Fig. 6 Comparison of *x*-velocities at the vertical centerline (R_e=10,000)

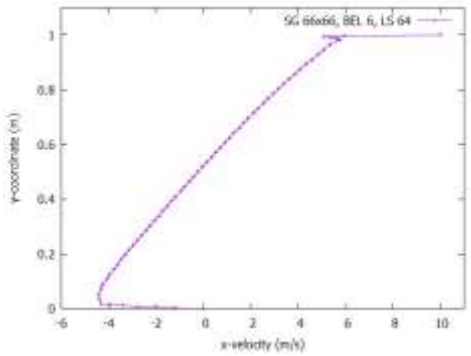

Fig. 7 Comparison of *x*-velocities at the vertical centerline (R_e=100,000)

REFERENCES

[1] U. Ghia, K.N. Ghia, and C. T. Shin, "High-Re solutions for incompressible flow using the Navier-Stokes equations and a multigrid method", Journal of Computational Physics, Vol. 48, 1982, pp. 387-411

[2] D.L. Logan, A First Course in Finite Element Method, 6th ed., Cengage Learning, 2015.